Hybrid-Mixed Stress Model for Reinforced Concrete with the Inclusion of a Bond Model

Tiago Daniel Schclar Leitão
Instituto Superior Técnico, Lisbon, Portugal

Summary

Following from previous research, the aim of this paper is to present a hybrid-mixed stress finite element model for the analysis of reinforced concrete, taking into account the bond between the concrete and the steel reinforcement. The finite element formulation is based on the independent approximation of the stress fields both in the concrete and steel domain, the displacement fields in the domain and static boundaries of concrete and steel, as well as the bond stress and slip in the concrete-steel interface. The latter two fields allow for the implementation of a non-linear bond response based on the model proposed by Mendes and Castro [1]. As verification, two examples based on previous experimental work are presented - pull-out test and reinforced concrete tie - supporting the assessment of the behaviour of both short and long anchorage lengths. The analyses adopt an incremental-iterative procedure, along with Legendre polynomials as approximation functions. The obtained results afford an adequate response, corroborating the employment of a hybrid-mixed stress model for reinforced concrete in conjunction with a bond model.

Keywords: Finite Elements, Reinforced Concrete, Hybrid-Mixed Stress Model, Concrete-Steel Bond, Physically Nonlinear Analysis

1 Introduction

The purpose of this paper is to apply the hybrid-mixed stress finite element formulation to the modelling of reinforced concrete considering concrete-steel bond behaviour. This formulation is included in the non-conventional finite element formulations, as opposed to the conventional displacement finite element model.

The hybrid-mixed stress model is one of the hybrid and mixed formulations developed by Freitas *et al.* [2] following previous work by Pian (1967) and Veubeke (1965). Three different formulations are proposed by the authors - hybrid-mixed, hybrid and hybrid-Trefftz. For each there are two different variants - the displacement and stress models. These formulations have useful characteristics, such as the use of hierarchical and independent approximations of stress and displacement (or deformation) fields, allowing great flexibility in the choice of shape functions, and the possibility to obtain quasi-statically admissible solutions. On the other hand, conventional finite element models, by approximating the displacement field, impose compatibility at a local level, though equilibrium is imposed in a weaker form, thus leading to kinematically admissible solutions.

The formulation used in the present work is part of the hybrid-mixed stress model. It is called hybrid due to the inclusion of independent approximation fields in the domain and on the boundaries and mixed as a result of approximating two different fields in the domain - stress and displacement. By approximating boundary displacements, there is a weighted imposition of boundary equilibrium, leading to the designation of stress model.

The extension of this method to reinforced concrete has been developed in previous works by the same research unit [3, 4, 5]. Adding a new level of detail in the finite element model comprises the consideration of steel-concrete bond behaviour. This property can be modelled by including an interface element that uses the bond model proposed by Mendes and Castro [1].

After a brief section stating the fundamental relations, the hybrid-mixed formulation for reinforced concrete, consisting of bidimensional concrete elements and linear reinforcement elements, is extended to include two new approximation fields - bond stress and slip. The inclusion of these approximations makes it possible to adapt the bond model proposed by Mendes and Castro [1]. The solving system will be able to include both linear and nonlinear concrete-reinforcement adherence behaviour. This formulation is then applied to two experimental cases that seek to evaluate its performance - a pull-out test and a reinforced concrete tie test.

The results were obtained using the program pyHM developed by Mendes and Castro [6], written in Python. MATLAB [7] was used to process the graphical results.

2 Fundamental relations

Considering a domain V, enclosed within a static boundary Γ_σ and a kinematic boundary Γ_u, the fundamental relations that govern the mechanical problem are [8, 2]:

$$\mathbf{D}\boldsymbol{\sigma} + \mathbf{b} = 0 \qquad \text{in } V \tag{1}$$
$$\boldsymbol{\varepsilon} = \mathbf{D}^*\mathbf{u} \qquad \text{in } V \tag{2}$$
$$\boldsymbol{\varepsilon} = \mathbf{F}\boldsymbol{\sigma} \qquad \text{in } V \tag{3}$$
$$\mathbf{N}\boldsymbol{\sigma} = \bar{\mathbf{t}} \qquad \text{on } \Gamma_\sigma \tag{4}$$
$$\mathbf{u} = \bar{\mathbf{u}} \qquad \text{on } \Gamma_u \tag{5}$$

Equations (1) and (2) define the equilibrium and compatibility conditions, where $\boldsymbol{\sigma}$ and $\boldsymbol{\varepsilon}$ list the independent components of the stress and strain fields, respectively, and $\mathbf{b}$ and $\mathbf{u}$ define the body forces and the displacement vector. $\mathbf{D}$ and $\mathbf{D}^*$ define the differential equilibrium and compatibility operators, which are linear and adjoint. The linear elastic constitutive relation (3), written in the flexibility format, associates the stress and strain fields through a flexibility matrix $\mathbf{F}$. Lastly, in the equilibrium and compatibility boundary conditions (4) and (5), respectively, $\bar{\mathbf{t}}$ are the external forces and $\bar{\mathbf{u}}$ the prescribed displacements, while $\mathbf{N}$ identifies the matrix containing the elements of the unit vector normal to the boundary.

3 Bond model

The transfer of longitudinal stresses between the reinforcement and the surrounding concrete occurs through the bond stresses - τ_b - at the concrete-steel interface V_i. The stress changes along the length of both materials causes strain differentials and, consequently, a relative displacement between the reinforcement and the concrete - slip $\mathbf{s}_b$ [9]. Thus, two fundamental equations are obtained:

$$\mathbf{s}_b = \mathbf{u}_{r,V} - \mathbf{u}_{c,\Gamma} \qquad \text{in } V_i \tag{6}$$
$$\tau_b = \mathbf{K}_s\mathbf{s}_b \qquad \text{in } V_i \tag{7}$$

where $\mathbf{u}_{r,V}$ and $\mathbf{u}_{c,\Gamma}$ define the steel domain displacement and the concrete displacement on the overlapping boundary. In the concrete-steel bond, the constitutive relation (7) is written in the stiffness format with the interface stiffness $\mathbf{K}_s$.

It is now possible to define the equilibrium both in the reinforcement domain (8) and on the concrete element boundary (9):

$$\mathbf{D}_r\overline{\mathbf{N}}_r + \mathbf{b}_r - \tau_b^* = 0 \qquad \text{in } V_r \tag{8}$$
$$\mathbf{N}_c\boldsymbol{\sigma}_c^* = \bar{\mathbf{t}}_c + \tau_b^* \qquad \text{on } \Gamma_{\sigma c} \tag{9}$$

where the index r identifies variables related to the reinforcement, $\overline{\mathbf{N}}_r$ is the steel axial tension, and c denotes variables related to concrete. It should be observed that, when imposing the interface equilibrium, only the relevant direction of the concrete operators is considered. As both equations are written in FL^{-1}, pseudo-stresses must be considered both for the bond stress, integrated along its perimeter $P_c = 2\pi r$ (where r is the reinforcement radius) and the concrete stress, integrated across its thickness e_c:

$$\tau_b^* = P_c k_s s_b \tag{10}$$
$$\boldsymbol{\sigma}_c^* = e_c\boldsymbol{\sigma}_c = e_c K_c\boldsymbol{\varepsilon}_c \tag{11}$$

Several bond models have been developed [9, 1]. This work uses the semi-analytical bond model proposed by Mendes and Castro [1]. Four main phases of bond behaviour must be considered: perfect bond, with a very high stiffness; with crack initiation there is a loss of chemical adhesion and a growth in slip; the widening of longitudinal cracks along the interface lead to a softening of the connection between the materials; lastly, for ribbed bars, the residual bond stress is guaranteed by friction.

The bond model is shown in Figure 1 and the parameters used to define the model are grouped in Table 1. The parameters are determined based on concrete-reinforcement bond experimental results.

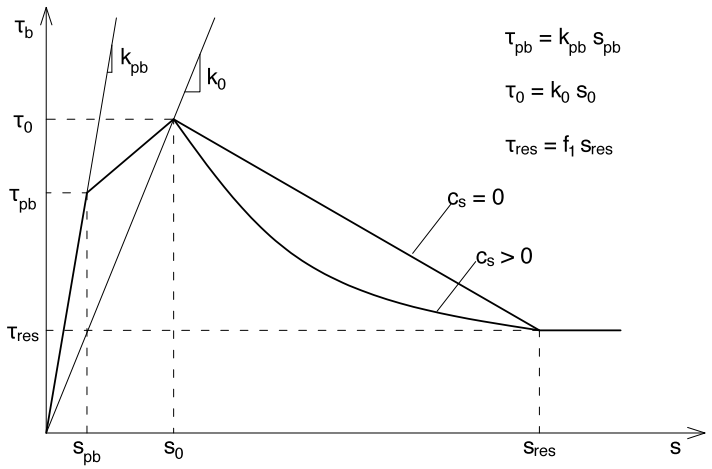

Figure 1: Bond model (adapted from Mendes and Castro [1])

Table 1: Bond model parameters (adapted from Mendes and Castro [1])

Parameter	Units	Definition
s_{pb}	L	perfect bond slip limit
s_0	L	slip at peak stress
s_{res}	L	slip at the begging of the residual stress
k_{pb}	FL^{-3}	Perfect bond tangent stiffness
k_0	FL^{-3}	Secant stiffness at peak stress
f_1	$-$	Residual stress ration
c_s	$-$	shape control parameter of the softening branch

4 Hybrid-mixed stress models

The hybrid-mixed stress model presented in this section derives from the model proposed by Freitas *et al.* [2]. That model was later adapted to reinforced concrete, considering plane stress concrete elements and bar elements for the reinforcement [5].

4.1 Approximation fields

For the concrete elements, three fields are approximated, namely the domain stresses $\boldsymbol{\sigma}_c$ and the domain and boundary displacements $\mathbf{u}_c$:

$$\boldsymbol{\sigma}_c = \mathbf{S}_c \mathbf{X}_c \qquad \text{in } V_c \tag{12}$$

$$\mathbf{u}_c = \mathbf{U}_{Vc} \mathbf{q}_{Vc} \qquad \text{in } V_c \tag{13}$$

$$\mathbf{u}_c = \mathbf{U}_{\Gamma c} \mathbf{q}_{\Gamma c} \qquad \text{on } \Gamma_{\sigma c} \tag{14}$$

For the reinforcement, the approximations include the domain axial tension $\overline{\mathbf{N}}_r$ and the domain and boundary displacements $\mathbf{u}_r$:

$$\overline{\mathbf{N}}_r = \mathbf{S}_r \mathbf{X}_r \qquad \text{in } V_r \tag{15}$$

$$\mathbf{u}_r = \mathbf{U}_{Vr} \mathbf{q}_{Vr} \qquad \text{in } V_r \tag{16}$$

$$\mathbf{u}_r = \mathbf{U}_{\Gamma r} \mathbf{q}_{\Gamma r} \qquad \text{on } \Gamma_{\sigma r} \tag{17}$$

Matrices $\mathbf{S}_c$, $\mathbf{U}_{Vc}$, $\mathbf{U}_{\Gamma c}$, $\mathbf{S}_r$, $\mathbf{U}_{Vr}$ and $\mathbf{U}_{\Gamma r}$ list the shape functions for each field and vectors $\mathbf{X}_c$, $\mathbf{q}_{Vc}$, $\mathbf{q}_{\Gamma c}$, $\mathbf{X}_r$, $\mathbf{q}_{Vr}$ and $\mathbf{q}_{\Gamma r}$ the corresponding weights.

For the interface element two fields must be considered - bond stress τ_b and slip s:

$$\tau_b = \mathbf{F}_b \boldsymbol{\lambda}_b \qquad \text{in } V_i \tag{18}$$

$$s = \mathbf{S}_b \mathbf{s}_b \qquad \text{in } V_i \tag{19}$$

where $\mathbf{F}_b$ and $\mathbf{S}_b$ list the shape functions and $\boldsymbol{\lambda}_b$ and $\mathbf{s}_b$ the corresponding weights.

It should be noted that both the concrete stress field and the bond stress are defined as pseudo-stresses, as explained in the previous section.

4.2 Finite element model

The fundamental relations must now be enforced in a weighed-residual approach. Equation (20) enforces the equilibrium (1) in the concrete domain and (24) the equilibrium in the bar domain (8), including the bond stress. Equations (21) and (25) impose the compatibility (2) in the concrete and steel domains, respectively, and (22) and (26) the linear elastic constitutive relations (3) for both materials. Lastly, equation (23) imposes the concrete boundary equilibrium (9), including the bond stress, and equation (27) imposes the reinforcement boundary equilibrium (4). Equations (21) and (25) are integrated by parts to accommodate the compatibility boundary conditions (5) both for concrete and reinforcement.

$$\int_{Vc} \mathbf{U}_{Vc}^T (\mathbf{D}_c \boldsymbol{\sigma}_c + \mathbf{b}_c)\, \mathrm{d}V_c = 0 \tag{20}$$

$$\int_{Vc} \mathbf{S}_c^T (\boldsymbol{\varepsilon}_c - \mathbf{D}_c^* \mathbf{u}_c)\, \mathrm{d}V_c = 0 \tag{21}$$

$$\int_{Vc} \mathbf{S}_c^T (\boldsymbol{\varepsilon}_c - \mathbf{F}_c \boldsymbol{\sigma}_c)\, \mathrm{d}V_c = 0 \tag{22}$$

$$\int_{\Gamma_{\sigma c}} \mathbf{U}_{\Gamma c}^T (\mathbf{N}_c \boldsymbol{\sigma}_c^* - \bar{\mathbf{t}}_c - \tau_b^*)\, \mathrm{d}\Gamma_{\sigma c} = 0 \tag{23}$$

$$\int_{Vr} \mathbf{U}_{Vr}^T (\mathbf{D}_r \overline{\mathbf{N}}_r + \mathbf{b}_r - \tau_b^*)\, \mathrm{d}V_r = 0 \tag{24}$$

$$\int_{Vr} \mathbf{S}_r^T (\boldsymbol{\varepsilon}_r - \mathbf{D}_r^* \mathbf{u}_r)\, \mathrm{d}V_r = 0 \tag{25}$$

$$\int_{Vr} \mathbf{S}_r^T (\boldsymbol{\varepsilon}_r - \mathbf{F}_r \overline{\mathbf{N}}_r)\, \mathrm{d}V_r = 0 \tag{26}$$

$$\int_{\Gamma_{\sigma r}} \mathbf{U}_{\Gamma r}^T (\mathbf{N}_r \overline{\mathbf{N}}_r - \bar{\mathbf{t}}_r)\, \mathrm{d}\Gamma_{\sigma r} = 0 \tag{27}$$

Regarding the interface elements, the enforcement of concrete-reinforcement displacement compatibility (6) and the elastic bond constitutive relation (7), equations (28) and (29), respectively, results in:

$$\int_{Vr} \mathbf{F}_b^T (s - \mathbf{u}_r + \mathbf{u}_c)\, \mathrm{d}V_r = 0 \tag{28}$$

$$\int_{Vr} \mathbf{S}_b^T (\tau_b^* - P_c k_s s)\, \mathrm{d}V_r = 0 \tag{29}$$

Inserting all the approximations defined in the previous section in the above equations, the resulting finite element equations give the governing system at the element level for the reinforced concrete hybrid-mixed stress model taking into account bond behaviour:

$$\begin{bmatrix} \mathbb{F}_c & 0 & \mathbf{A}_{Vc} & 0 & -\mathbf{A}_{\Gamma c} & 0 & 0 & 0 \\ 0 & \mathbb{F}_r & 0 & \mathbf{A}_{Vr} & 0 & -\mathbf{A}_{\Gamma r} & 0 & 0 \\ \mathbf{A}_{Vc}^T & 0 & 0 & 0 & 0 & 0 & 0 & 0 \\ 0 & \mathbf{A}_{Vr}^T & 0 & 0 & 0 & 0 & -\mathbf{C}_{br}^T & 0 \\ -\mathbf{A}_{\Gamma c}^T & 0 & 0 & 0 & 0 & 0 & \mathbf{C}_{bc}^T & 0 \\ 0 & -\mathbf{A}_{\Gamma r}^T & 0 & 0 & 0 & 0 & 0 & 0 \\ 0 & 0 & 0 & -\mathbf{C}_{br} & \mathbf{C}_{bc} & 0 & 0 & \mathbf{C}_{bs} \\ 0 & 0 & 0 & 0 & 0 & 0 & \mathbf{C}_{bs}^T & -\mathbf{K}_s \end{bmatrix} \begin{bmatrix} \mathbf{X}_c \\ \mathbf{X}_r \\ \mathbf{q}_{Vc} \\ \mathbf{q}_{Vr} \\ \mathbf{q}_{\Gamma c} \\ \mathbf{q}_{\Gamma r} \\ \boldsymbol{\lambda}_b \\ \mathbf{s}_b \end{bmatrix} = \begin{bmatrix} \bar{\mathbf{v}}_c \\ \bar{\mathbf{v}}_r \\ -\mathbf{Q}_{Vc} \\ -\mathbf{Q}_{Vr} \\ -\mathbf{Q}_{\Gamma c} \\ -\mathbf{Q}_{\Gamma r} \\ 0 \\ 0 \end{bmatrix} \tag{30}$$

The global solving system is equivalent to the elemental one. Elements of the same type are connected by considering the same approximation for the inter-element boundary displacement field. Hence, apart from the boundary operators (with index Γ), all the others are totally independent for each element, not occurring any overlap in the global system. Detailed construction of a solving system may be found in [10, 11].

The solving system operators are derived in [12]. The operators related to either concrete or reinforcement are defined by the following expressions:

$$\mathbb{F}_c = \int_{Vc} \mathbf{S}_c^T \mathbf{F}_c \mathbf{S}_c \, \mathrm{d}V_c \tag{31}$$

$$\mathbf{A}_{Vc} = \int_{Vc} (\mathbf{D}_c \mathbf{S}_c)^T \mathbf{U}_{Vc} \, \mathrm{d}V_c \tag{32}$$

$$\mathbf{A}_{\Gamma c} = \int_{\Gamma_{\sigma c}} (\mathbf{N}_c \mathbf{S}_c)^T \mathbf{U}_{\Gamma c} \, \mathrm{d}\Gamma_{\sigma c} \tag{33}$$

$$\mathbf{Q}_{Vc} = \int_{Vc} \mathbf{U}_{Vc}^T \mathbf{b}_c \, \mathrm{d}V_c \tag{34}$$

$$\mathbf{Q}_{\Gamma c} = \int_{\Gamma_{\sigma c}} \mathbf{U}_{\Gamma c}^T \bar{\mathbf{t}}_c \, \mathrm{d}\Gamma_{\sigma c} \tag{35}$$

$$\bar{\mathbf{v}}_c = \int_{\Gamma_{uc}} (\mathbf{N}_c \mathbf{S}_c)^T \bar{\mathbf{u}}_c \, \mathrm{d}\Gamma_{uc} \tag{36}$$

$$\mathbb{F}_r = \int_{Vr} \mathbf{S}_r^T \mathbf{F}_r \mathbf{S}_r \, \mathrm{d}V_r \tag{37}$$

$$\mathbf{A}_{Vr} = \int_{Vr} (\mathbf{D}_r \mathbf{S}_r)^T \mathbf{U}_{Vr} \, \mathrm{d}V_r \tag{38}$$

$$\mathbf{A}_{\Gamma r} = \int_{\Gamma_{\sigma r}} (\mathbf{N}_r \mathbf{S}_r)^T \mathbf{U}_{\Gamma r} \, \mathrm{d}\Gamma_{\sigma r} \tag{39}$$

$$\mathbf{Q}_{Vr} = \int_{Vr} \mathbf{U}_{Vr}^T \mathbf{b}_r \, \mathrm{d}V_r \tag{40}$$

$$\mathbf{Q}_{\Gamma r} = \int_{\Gamma_{\sigma r}} \mathbf{U}_{\Gamma r}^T \bar{\mathbf{t}}_r \, \mathrm{d}\Gamma_{\sigma r} \tag{41}$$

$$\bar{\mathbf{v}}_r = \int_{\Gamma_{ur}} (\mathbf{N}_r \mathbf{S}_r)^T \bar{\mathbf{u}}_r \, \mathrm{d}\Gamma_{ur} \tag{42}$$

The operators linked with the concrete-reinforcement interface are given by:

$$\mathbf{C}_{bc} = \int_{Vr} \mathbf{F}_b^T \mathbf{U}_{\Gamma c} \, \mathrm{d}V_r \tag{43}$$

$$\mathbf{C}_{br} = \int_{Vr} \mathbf{F}_b^T \mathbf{U}_{Vr} \, \mathrm{d}V_r \tag{44}$$

$$\mathbf{C}_{bs} = \int_{Vr} \mathbf{F}_b^T \mathbf{S}_b \, \mathrm{d}V_r \tag{45}$$

$$\mathbf{K}_s = \int_{Vr} \mathbf{S}_b^T P_c k_s \mathbf{S}_b \, \mathrm{d}V_r \tag{46}$$

4.3 Nonlinear behaviour

Because the bond model is nonlinear, to solve the governing system it is necessary to adopt an incremental-iterative resolution method (Newton-Raphson). For each load increment, there is an iterative process in order to reduce the error to an acceptable level [13].

Considering an interface tangent stiffness k_s^* the new stiffness operator may be obtained by the expression:

$$\mathbf{K}_s^* = \int_{Vr} \mathbf{S}_b^T P_c k_s^* \mathbf{S}_b \, \mathrm{d}V_r \tag{47}$$

At the end of each iteration, the error is given by:

$$\begin{bmatrix} R_{X_c} \\ R_{X_r} \\ R_{q_{Vc}} \\ R_{q_{Vr}} \\ R_{q_{\Gamma c}} \\ R_{q_{\Gamma r}} \\ R_{\lambda_b} \\ R_{\mathbf{s}_b} \end{bmatrix} = \begin{bmatrix} 0 \\ 0 \\ 0 \\ 0 \\ 0 \\ 0 \\ 0 \\ -\mathbf{t}_b \end{bmatrix} + \begin{bmatrix} \mathbb{F}_c & 0 & \mathbf{A}_{Vc} & 0 & -\mathbf{A}_{\Gamma c} & 0 & 0 & 0 \\ 0 & \mathbb{F}_r & 0 & \mathbf{A}_{Vr} & 0 & -\mathbf{A}_{\Gamma r} & 0 & 0 \\ \mathbf{A}_{Vc}^T & 0 & 0 & 0 & 0 & 0 & 0 & 0 \\ 0 & \mathbf{A}_{Vr}^T & 0 & 0 & 0 & 0 & -\mathbf{C}_{br}^T & 0 \\ -\mathbf{A}_{\Gamma c}^T & 0 & 0 & 0 & 0 & 0 & \mathbf{C}_{bc}^T & 0 \\ 0 & -\mathbf{A}_{\Gamma r}^T & 0 & 0 & 0 & 0 & 0 & 0 \\ 0 & 0 & 0 & -\mathbf{C}_{br} & \mathbf{C}_{bc} & 0 & 0 & \mathbf{C}_{bs} \\ 0 & 0 & 0 & 0 & 0 & 0 & \mathbf{C}_{bs}^T & 0 \end{bmatrix} \begin{bmatrix} \mathbf{X}_c \\ \mathbf{X}_r \\ \mathbf{q}_{Vc} \\ \mathbf{q}_{Vr} \\ \mathbf{q}_{\Gamma c} \\ \mathbf{q}_{\Gamma r} \\ \boldsymbol{\lambda}_b \\ \mathbf{s}_b \end{bmatrix} - \begin{bmatrix} \bar{\mathbf{v}}_c \\ \bar{\mathbf{v}}_r \\ -\mathbf{Q}_{Vc} \\ -\mathbf{Q}_{Vr} \\ -\mathbf{Q}_{\Gamma c} \\ -\mathbf{Q}_{\Gamma r} \\ 0 \\ 0 \end{bmatrix} \tag{48}$$

For each iteration, as long as the error is not smaller than a given tolerance, the increments to the independent variables is obtained by:

$$\begin{bmatrix} \mathbb{F}_c & 0 & \mathbf{A}_{Vc} & 0 & -\mathbf{A}_{\Gamma c} & 0 & 0 & 0 \\ 0 & \mathbb{F}_r & 0 & \mathbf{A}_{Vr} & 0 & -\mathbf{A}_{\Gamma r} & 0 & 0 \\ \mathbf{A}_{Vc}^T & 0 & 0 & 0 & 0 & 0 & 0 & 0 \\ 0 & \mathbf{A}_{Vr}^T & 0 & 0 & 0 & 0 & -\mathbf{C}_{br}^T & 0 \\ -\mathbf{A}_{\Gamma c}^T & 0 & 0 & 0 & 0 & 0 & \mathbf{C}_{bc}^T & 0 \\ 0 & -\mathbf{A}_{\Gamma r}^T & 0 & 0 & 0 & 0 & 0 & 0 \\ 0 & 0 & 0 & -\mathbf{C}_{br} & \mathbf{C}_{bc} & 0 & 0 & \mathbf{C}_{bs} \\ 0 & 0 & 0 & 0 & 0 & 0 & \mathbf{C}_{bs}^T & -\mathbf{K}_s^* \end{bmatrix} \begin{bmatrix} \Delta\mathbf{X}_c \\ \Delta\mathbf{X}_r \\ \Delta\mathbf{q}_{Vc} \\ \Delta\mathbf{q}_{Vr} \\ \Delta\mathbf{q}_{\Gamma c} \\ \Delta\mathbf{q}_{\Gamma r} \\ \Delta\boldsymbol{\lambda}_b \\ \Delta\mathbf{s}_b \end{bmatrix} = - \begin{bmatrix} R_{X_c} \\ R_{X_r} \\ R_{q_{Vc}} \\ R_{q_{Vr}} \\ R_{q_{\Gamma c}} \\ R_{q_{\Gamma r}} \\ R_{\lambda_b} \\ R_{s_b} \end{bmatrix} \tag{49}$$

5 Numerical tests

Two examples based on previous experimental work are shown here in order to evaluate the response and accuracy of the proposed model.

The interface element is placed in parallel, that is, it is superimposed on the concrete boundary, connecting it with the reinforcement element.

Because of the properties of orthogonal functions, Legendre polynomials were used as approximation functions, allowing for highly sparse and numerically efficient governing systems[14].

5.1 Example 1 - Pull-out tests by Eligehausen *et al.* [15]

This example is a pull-out test, consisting of a ribbed reinforcement bar embedded in a concrete specimen, disconnected near both edges, as shown in Figure 2a. Loading is imposed using controlled displacements on the left protruding end of the reinforcement

As a result of a $5\phi_s$ concrete-steel contact length, the specimen is considered short, in terms of the anchorage length. Due to the small anchorage length, stress transfers will occur along the total breadth of the interface. Therefore, the specimen is expected to display near uniform distributions of bond stress and slip.

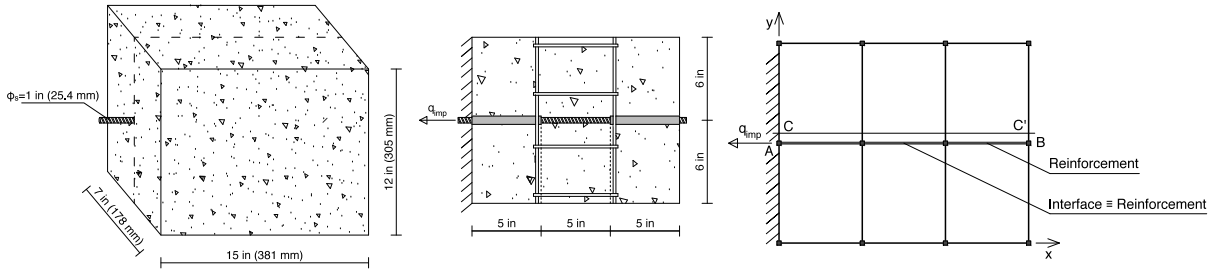

(a) Geometric characteristics

(b) Finite element mesh

Figure 2: Geometric characteristics and the finite element mesh used in the analyses

The mesh used is shown in Figure 2b and the values used to define all the material properties are stated in Table 2.

Table 2: Material properties (adapted from Mendes and Castro [1])

Material	Properties
Concrete	$E_c = 30.5\,\text{GPa} \quad \nu = 0.20 \quad t_c = 178\,\text{mm}$
Reinforcement	$E_r = 200.0\,\text{GPa} \quad \nu = 0.30 \quad A_r = 5.067\,\text{cm}^2$ $(\phi_s = 25.4\,\text{mm})$
Interface	$k_{pb} = 32.94\,\text{GPa/m} \quad k_0 = 8.235\,\text{GPa/m} \quad f_1 = 0.35 \quad c_s = 0.00$ $s_{pb} = 0.343\,\text{mm} \quad s_0 = 1.70\,\text{mm} \quad s_{res} = 10.50\,\text{mm}$

Adopting stress and tension fields approximation degrees of $n_x = 10$ and the other approximation degrees with values $n_x - 1 = 9$, the model has a total of 3786 degrees of freedom. Loading consisted of a displacement q_{imp} imposed as shown in Figure 2b, applied in 120 steps of 0.1 mm, up to a maximum total value of 12.00 mm.

Figure 3 shows the bond stress in relation to the displacement measured at point B. Because the bond stress is not entirely uniform along the interface, an equivalent bond stress $\tau_b^{eq} = Q_c/A_c$ was considered, where Q_c is the constraint force at point A due to the imposed displacement and A_c the total surface area of the reinforcement bar connected to the concrete ($A_c = P_c L_c$). In the same figure are included the experimental results obtained by Eligehausen *et al.* [15] and the conventional finite element analysis executed by Mendes and Castro [1]. It clearly shows that both finite element analyses reach very similar results, confirming the suitability of the hybrid-mixed stress formulation to model bond behaviour. Also, considering the values proposed by Mendes and Castro [1], the bond model provides a good approximation of the observed experimental behaviour.

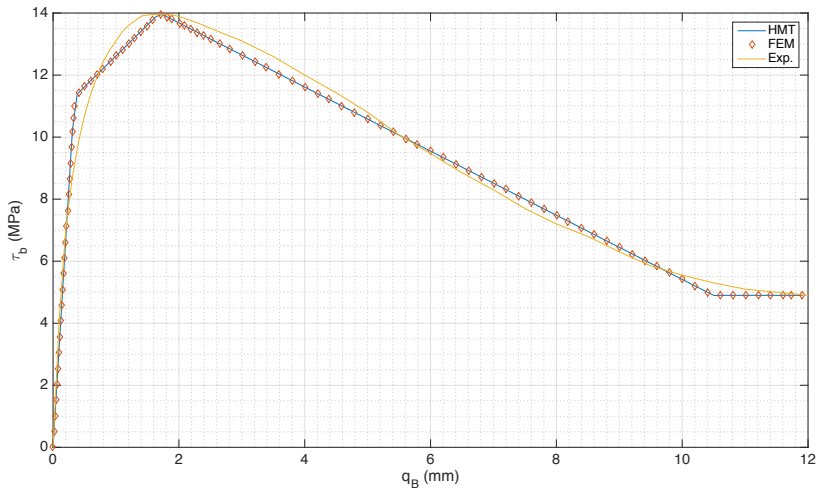

Figure 3: Bond stress vs. displacement at point B (experimental data from Eligehausen *et al.* [15] and conventional FEM results from Mendes and Castro [1])

The bond stress distribution at selected load steps is shown in Figure 4. In the first step (0.1 mm), the interface is still in the initial high stiffness branch shown in Figure 1. This means a very small change in slip leads to a significant change in the bond stress, explaining the non uniform distribution shown in the figure - as the stress transfer occurs between steel and concrete, the slip changes, thus altering the bond stress. For the fifth step ($q_{imp} = 0.5$ mm), the first part of the interface, closer to the loading point, is at the second branch of the bond behaviour diagram (Figure 1), whereas the rest of the interface is still in the high stiffness branch. Therefore, the first part shows a significant loss of sensibility to the change in slip, displaying a uniform distribution. The other two steps - $q_{imp} = 2.0$ mm, near peak bond stress, and $q_{imp} = 12.0$ mm, at the residual stress phase - feature a near uniform distribution of stresses, as expected.

Another relevant result is shown in Figure 5, for $q_{imp} = 2.0$ mm. It displays the reinforcement stress distribution together with the concrete σ_{xx} stresses at section $A - B$ ($y = 152.40$ mm) and section $C - C'$ ($y = 167.75$ mm). At first inspection, it can be seen that the concrete and steel stresses along the interface zone show a linear variation, in agreement with a uniform bond stress transfer. Additionaly, the first reinforcement element displays a constant stress, as there is no connection to the surrounding concrete elements, the last reinforcement element has no stresses, respecting equilibrium conditions. The figure also shows a significant concrete stress cluster at both ends of the interface element. However, plotting the concrete stress distribution just 15 mm apart from the interface presents a much smoother transition of stresses in those areas.

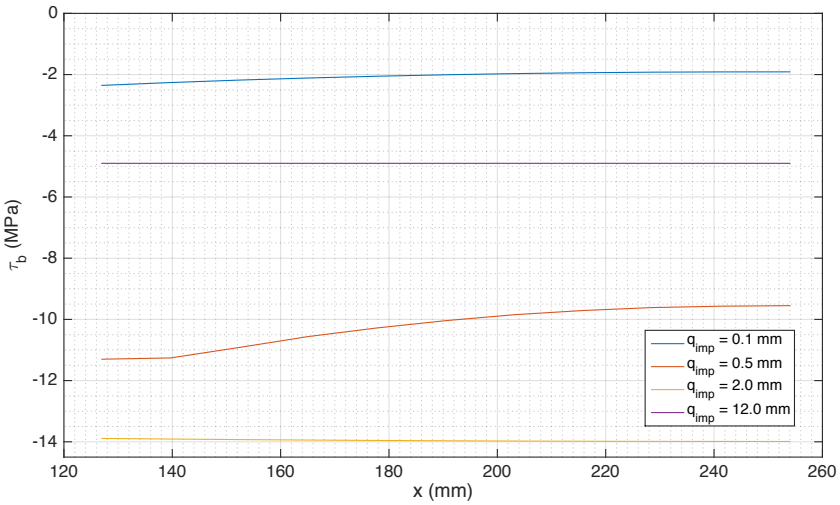

Figure 4: Bond stress distribution at selected load steps

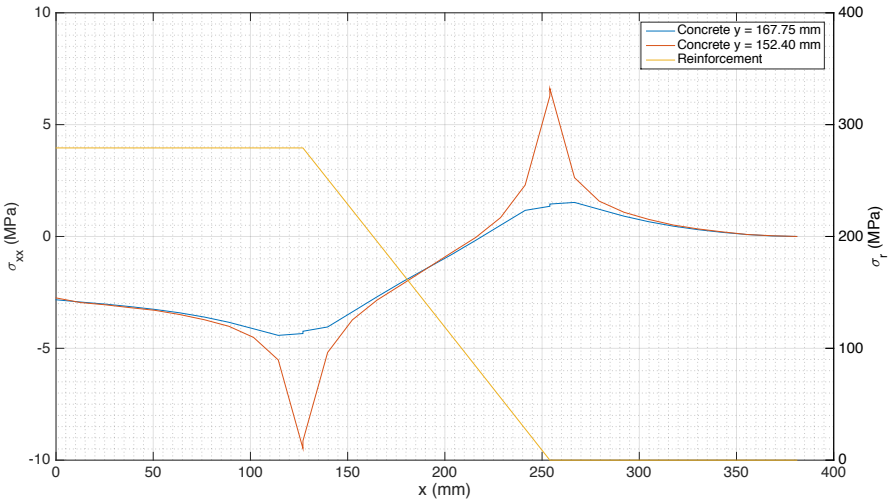

Figure 5: Concrete (σ_{xx}) and reinforcement stress distributions for $q_{imp} = 2.0\,\text{mm}$

5.2 Example 2 - RC tie tests by Clément [16]

This example consists of a reinforced concrete tie with symmetrically imposed displacements on both ends of the reinforcement. The geometric characteristics are shown in Figure 6. The mesh used in the analyses is displayed in Figure 7, together with the restraint conditions applied. As can be observed, the mesh comprises four bidimensional concrete elements and two reinforcement elements, each connected to the concrete by an interface element.

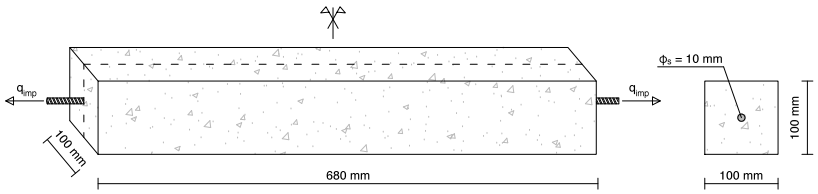

Figure 6: Geometric characteristics of tests performed by Clément [16] (adapted from Mendes [17])

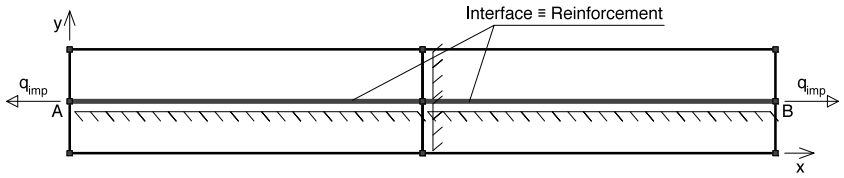

Figure 7: Finite element mesh for Example 2

The material parameters can be found in Table 3. Both for concrete and steel a linear elastic behaviour was considered. Due to lack of detailed information on the bond behaviour, the approach followed by Mendes [17] was adopted, thus considering a linear behaviour for the interface, with a constant stiffness values in a range coherent with the experimental results. A more detailed explanation may be found in [12].

This example considers a specimen that can be classified as medium/long. Therefore, it is expected to result in a balancing of the concrete and steel strains in part of the specimen, as a length segment of the interface should show no stress transfer. It should also be stated that the tie displays a similar behaviour to the tensioned section of a beam, thus providing results that may be relevant to practical applications.

Several approximation degrees were tested [12] and the set that provided the best results were a high degree for the concrete and steel stresses, $n_x = 20$, coupled with significantly lower degrees fro the rest of the approximations, $n_{uv} = n_{u\Gamma} = n_\tau = n_s) = 12$. The resulting model has 7028 degrees of freedom.

Table 3: Material parameters (adapted from Mendes [17])

Material	Parameters
Concrete	$E_c = 30.5\,\text{GPa} \quad \nu = 0.20 \quad t_c = 178\,\text{mm}$
Reinforcement	$E_r = 210.0\,\text{GPa} \quad \nu = 0.30 \quad A_r = 78.5398\,\text{mm}^2\ (\phi_s = 10\,\text{mm})$
Interface	$k_s = \{0, 60, 120, 240\}\text{GPa/m}$

Because there is no non-linearity in the solving system, no incremental-iterative has to be considered. Therefore, two symmetrical displacements were imposed, with values $q_{imp} = 0.125\,\text{mm}$, totalling a controlled displacement $\Delta q_{imp} = 0.25\,\text{mm}$.

Figures 8a and 8b show the steel stresses and concrete σ_{xx} stress distribution at $y = 50\,\text{mm}$ (section $A - B$). As expected, the higher the interface stiffness, the larger the central area of uniform stresses. This implies that there is no stress transfer in the central area, confirmed by the null bond stresses displayed in Figure 9a. Accordingly, higher values of k_s result in higher stress slopes in the specimen ends, because there is a larger stress transfer capacity per length of interface. The lowest value of interface stiffness, i.e. $k_s = 0\,\text{GPa/m}$, implies a lack of connection between both materials, thus resulting in zero bond stress and, consequently, zero concrete stresses. Figure 9b shows that with the increase in bond stiffness, there is a decrease in the maximum slip. The extreme case, of perfect bond, would lead to no slip. On the other end, for $k_s = 0\,\text{GPa/m}$, the slip equals the bar extension due to tension.

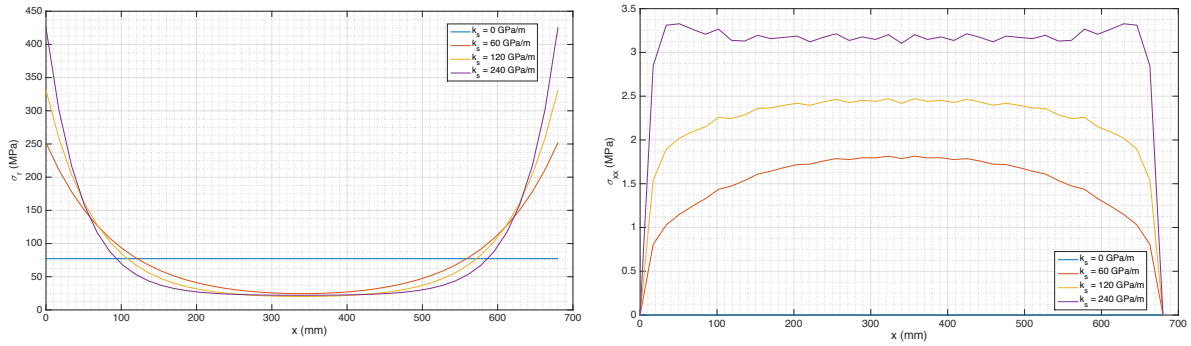

(a) Reinforcement stress

(b) Concrete σ_{xx} stress

Figure 8: Reinforcement and concrete stresses for $\Delta q_{imp} = 0.25\,\text{mm}$

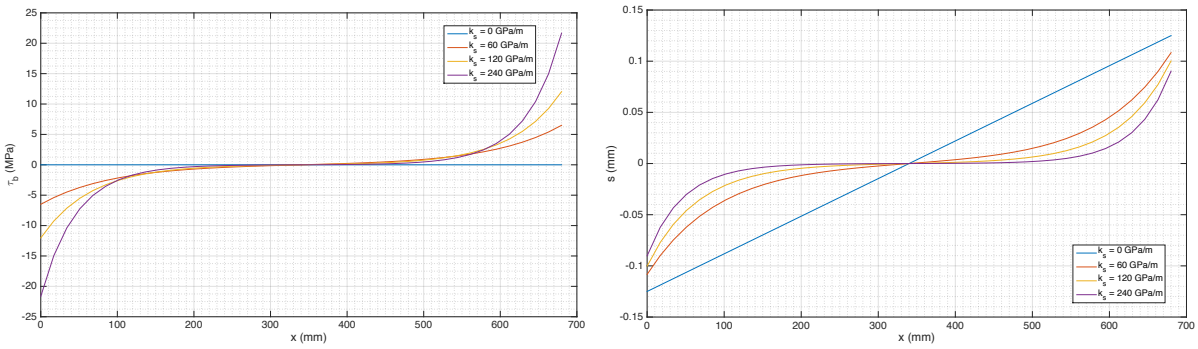

(a) Bond stress

(b) Bond slip

Figure 9: Bond stress and slip for $\Delta q_{imp} = 0.25\,\text{mm}$

6 Closure

The scope of the present work was to advance previous research on non-conventional finite element formulations. The main aim was to extend the hybrid-mixed stress formulation in order to model reinforced concrete

considering bond behaviour. Having the reinforced concrete hybrid-mixed model, considering bidimensional concrete elements and bar reinforcement elements, as a starting point, the purpose of this work was to include the bond model proposed by Mendes and Castro [1] by introducing new approximation fields for the bond stress and slip in the interface between both materials.

In order to evaluate the performance of the proposed model, two examples were analysed, which focus was the study of the concrete-reinforcement connection. The main conclusions are as follows:

- The HMT model lends itself to the modelling of reinforced concrete with steel-concrete bond failure, giving satisfactory results that are in accordance with those obtained in laboratory tests;
- The consideration of the physical nonlinearity of the bond behaviour is effectively modelled by adopting an incremental-iterative method (Newton-Raphson);
- Taking into account the loss of bond between the two materials affects the overall results, when compared with the consideration of a perfect bond;
- The use of Legendre polynomials as shape functions leads to results consistent with the expected distributions in experimental works, except for a few singularity points (especially at the extremities of the interface elements).

6.1 Future work

Future work may include:

- Coupling of HMT formulation simultaneously with concrete physical nonlinearity (damage model) and concrete-reinforcement bond nonlinearity (bond model);
- Extending the formulation to two-dimensional structures of greater complexity (e.g., inclusion of transverse reinforcement) and to three-dimensional structures;
- Application of cyclic and dynamic loading;
- Consistent and methodical evaluation of the decision process about the approximation degrees.
- Inclusion of fracture mechanics to model the concrete behaviour.

References

[1] L. A. M. Mendes and L. M. S. S. Castro, "A new rc bond model suitable for three-dimensional cyclic analyses", *Computers and Structures*, vol. 120, pp. 47–64, 2013.

[2] J. T. Freitas, J. M. de Almeida and E. R. Pereira, "Non-conventional formulations for the finite element method", *Computational Mechanics*, vol. 23, no. 5-6, pp. 488–501, 1999.

[3] C. M. Silva and L. M. S. S. Castro, "Hybrid-mixed stress formulation using continuum damage models", *Communications in Numerical Methods in Engineering*, vol. 22, pp. 605–617, 2006.

[4] M. R. T. Arruda and L. M. S. S. Castro, "A new hybrid-mixed stress model for the analysis of concrete structures using damage mechanics", *Computers and Structures*, vol. 125, pp. 23–44, 2013.

[5] M. F. S. Luz, "Modelos híbridos-mistos de tensão para a análise de estruturas de betão armado", Master's thesis, Instituto Superior Técnico, Lisboa, 2013.

[6] L. Mendes and L. Castro, "Pyhm - python-based hybrid-mixed finite element code", Relatório ICIST, 2016.

[7] MATLAB, *MATLAB Release 2015a*. Natick, Massachusetts, United States: The MathWorks, Inc., 2015.

[8] O. Pereira, "Um modelo de elementos finitos de equilíbrio para elasticidade tridimensional", Master's thesis, Instituto Superior Técnico, Lisboa, 1993.

[9] FIB, *Bond of reinforcement in concrete*, ser. State-of-art report. Lausanne, Switzerland: International Federation for Structural Concrete (FIB), 2000, vol. Bulletin 10.

[10] L. M. S. S. Castro, "Wavelets e séries de walsh em elementos finitos", PhD thesis, Instituto Superior Técnico, Lisboa, 1996.

[11] L. A. M. Mendes, "Modelos de elementos finitos híbridos-mistos de tensão na análise elastoplástica de estruturas laminares planas", Master's thesis, Instituto Superior Técnico, Lisboa, 2002.

[12] T. D. S. Leitão, "Modelos híbridos-mistos de tensão - Simulação da perda de aderência aço-betão em estruturas de betão armado", Master's thesis, Instituto Superior Técnico, Lisboa, 2016.

[13] DIANA, *DIANA-9.43 User's Manual - Analysis Procedures*, 1st ed., J. Manie and W. P. Kikstra, Eds. The Netherlands: TNO DIANA BV, 2010.

[14] E. M. B. R. Pereira and J. A. T. Freitas, "A mixed-hybrid finite element model based on orthogonal functions", *International journal for numerical methods in engineering*, vol. 39, pp. 1295–1312, 1996.

[15] R. Eligehausen, E. P. Popov and V. V. Bertero, "Local bond stress-slip relationships of deformed bars under generalized excitations", Earthquake Engineering Research Center, University of California, Berkeley, USA, Report UCB/EERC 83/23, 1983.

[16] J. L. Clément, "Interface acier-béton et comportement des structures en béton armé: Caractérisation, modélisation", PhD thesis, Université Paris VI, Paris, 1987.

[17] L. A. M. Mendes, "Refined three-dimensional seismic analysis of reinforced concrete structures", PhD thesis, Instituto Superior Técnico, Lisboa, 2011.